

## LENSING OPTICAL DEPTHS FOR SUBSTRUCTURE AND ISOLATED DARK MATTER HALOS

JACQUELINE CHEN, ANDREY V. KRAVTSOV & CHARLES R. KEETON<sup>1</sup>

Department of Astronomy & Astrophysics, Center for Cosmological Physics, The University of Chicago,  
5640 S. Ellis Ave., Chicago, IL 60637  
*Draft version November 12, 2018*

### ABSTRACT

Multiply-imaged quasar lenses can be used to constrain the substructure mass fraction in galaxy-sized dark matter halos via anomalous flux ratios in lensed images. The flux ratios, however, can be affected by both the substructure in the lens halo and by isolated small-mass halos along the entire line-of-sight to the lensed source. While lensing by dark matter clumps near the lens galaxy is more efficient than elsewhere, the cumulative effect of all objects along the line-of-sight could be significant. Here we estimate the potential contribution of isolated clumps to the substructure lensing signal using a simple model motivated by cosmological simulations. We find that the contribution of isolated clumps to the total lensing optical depth ranges from a few to tens percent, depending on assumptions and the particular configuration of the lens. Therefore, although the contribution of isolated clumps to the lensing signal is not dominant, it should not be neglected in detailed analyses of substructure lensing. For the currently favored  $\Lambda$ CDM model, the total calculated optical depth for lensing is high,  $\tau \sim 0.2 - 20$  and could, therefore, naturally explain the high frequency of anomalous flux ratios in observed lenses. The prediction, however, is highly sensitive to the spatial distribution of substructure halos in the innermost regions of the lens halo, which is still very uncertain. Therefore, constraints on the properties of the substructure population or accurate cosmological constraints, such as the mass of the warm dark matter particle, are difficult if not impossible to derive at this point.

*Subject headings:* gravitational lensing – cosmology: theory – dark matter

### 1. INTRODUCTION

One of the generic predictions of the Cold Dark Matter (CDM) paradigm is a “clumpy” distribution of matter, with a large number of small-mass compact dark matter (DM) halos, both within virialized regions of larger halos (substructure) and in the field. At the same time, the observed number of dwarf galaxy satellites in the Local Group is more than an order of magnitude smaller than expected (Klypin et al. 1999b; Moore et al. 1999). This discrepancy has motivated many theoretical studies of alternative models designed to reduce the abundance of substructure (e.g., Spitzer & Steinhardt 2000; Hanesstet & Scherrer 2000; Hu et al. 2000) or to suppress star formation in small clumps via astrophysical mechanisms, making them dark (Bullock et al. 2000; Benson et al. 2002; Somerville 2002).

If the CDM paradigm is correct, we expect  $\sim 2 - 10\%$  of the mass of a present-day galactic halo to be tied up in substructure (e.g., Klypin et al. 1999b; Ghigna et al. 2000; Kravtsov et al. 2003). The absence of apparent optical counterparts would then indicate that the small-mass DM clumps are dark. In the future, it may be possible to detect substructure using different methods: for example, indirectly via the effect of clumpy matter distributions on tidal tails of satellite galaxies (Mayer et al. 2002) or directly via annihilation or other observable signatures (e.g., Bergström et al. 1999; Tasitsiomi & Olinto 2002, and references therein). At the current time, however, gravitational lensing represents the best avenue to constraining populations of DM clumps in galactic halos (Mao & Schneider 1998; Metcalf & Madau 2001; Dalal & Kochanek 2002; Metcalf & Zhao 2002). This is because substructure can modify the fluxes of lensed images relative to those

predicted by smooth lens models. The existence of such anomalous fluxes in many lens systems has been known for some time (Mao & Schneider 1998). Recently, several such systems were analyzed with the goal of constraining the properties of substructure in lens halos. Dalal & Kochanek (2002) carried out a statistical study of seven radio lenses and found that the halo mass fraction in substructure,  $f_{\text{sub}}$ , is approximately  $\sim 2 - 5\%$  (see Evans & Witt 2003, for an alternative interpretation). This number is broadly consistent with the typical substructure fractions of  $\sim 0.02 - 0.1$  predicted by numerical simulations of CDM models (Kravtsov et al. 2003). Note, however, that predicted fractions are for the total substructure populations within the virial radius, while lensing observations are sensitive only to substructure in a cylinder of radius  $\sim 5 - 10$  kpc around the lens center. In addition, the abundance of clumps and their mass fraction can be expected to be depressed in the central regions due to increased tidal disruption and merging.

Dalal & Kochanek (2002) and all other authors who have studied substructure lensing have assumed that the lensing is caused only by clumps in the halo of the lens galaxy. CDM models, however, predict that large numbers of small-mass clumps also exist in the field around galactic halos (e.g., Sheth & Tormen 1999; Klypin et al. 1999b). Although the lensing efficiency of an individual field clump is expected to be low, a typical path length from the source quasar may intersect the Einstein radii of many field clumps, resulting in a significant optical depth relative to that of substructure lensing. Indeed, Keeton (2003) recently showed that the lensing efficiency for DM clumps, as a function of redshift, peaks at the redshift of the lens but is fairly wide ( $\Delta z \sim 0.3 - 0.5$ ) and has tails that extend to the redshifts of the observer and of the source. Thus, the cumulative effect of all small-mass

<sup>1</sup> Hubble Fellow

DM clumps along the line-of-sight to the source could be significant. In this paper, we use a simple analytic model motivated by the results of cosmological simulations to estimate and compare the optical depth for lensing by substructure to that of the isolated ‘field’ halos. We apply the model to two specific strong lens systems, B1422+231 and PG 1115+080, with anomalous flux ratios and present our conclusions for these systems.

The paper is organized as follows. In section §2, we summarize the formalism of Keeton (2003), used to calculate the lensing optical depth of individual DM clumps. We describe the model for the spatial and mass distributions of satellite and isolated DM halos in § 3. § 4 contains the main details for the two observed lens systems that we analyze. Finally, we present our results and conclusions in § 5 and 6.

## 2. OPTICAL DEPTH

The goal of this study is to compare the lensing efficiency of substructure located within the lens halo to that of clumps along the line-of-sight and in the immediate vicinity (but outside) the lens. We do this by comparing the optical depth, a measure of the lensing probability, of the two populations. The formalism for computing the lensing optical depth for small DM clumps in a strong lens system was recently derived by Keeton (2003) and we refer the reader to this paper for further details. In this section we summarize the main equations used in our calculations.

Since we are concerned with spatially small perturbations to a large smooth gravitational lens, we assume that lensing cross sections can be calculated by treating the lens as an external field. The cross-section for lensing by clumps is calculated assuming that their density distributions can be described by singular isothermal spheres (SISs). As the effect of clump lensing can vary from negligible to very strong, we restrict ourselves to a minimum threshold effect on image flux (i.e., magnification or demagnification). To this end, we estimate the cross section by taking into account all instances where the magnification or de-magnification by a clump is larger than a threshold value  $\delta$ . We then calculate the total optical depth for clump lensing by integrating the cross section over the clump mass function in a given patch of sky and dividing by the area of the patch:

$$\tau(\delta; \kappa, \gamma) = \int dz D(z)^2 \frac{dD}{dz} \int dM \frac{dn}{dM} \sigma(\delta; \kappa, \gamma, \beta, M), \quad (1)$$

where  $\kappa$  and  $\gamma$  are the convergence and shear of the image and  $D(z)$  is the comoving distance.  $\beta$  parameterizes the distance ratios between the clump and the halo, so that in the situation where the  $z_1$  is the redshift of the object closer to the observer and  $z_2$  is the redshift of the further object,

$$\beta = \frac{D_{12} D_{os}}{D_{o2} D_{1s}}, \quad (2)$$

where  $D_{ij} = D(z_i, z_j)$  and  $o$  and  $s$  refer to the observer and source redshift, respectively.

An estimate of the cross section for a general line-of-sight clump is given by the effective area  $A$  of the “ $\delta$ -curve”, the curve in the source plane where all images have magnification  $\mu = (1 + \delta)\mu_0$ , compared to the unperturbed

magnification

$$\mu_0 = [(1 - \kappa)^2 - \gamma^2]^{-1}. \quad (3)$$

This estimate gives the exact cross section for configurations where the clump does not change the number of lensed images, and a good approximation (usually a lower limit) for configurations where the clump creates additional faint, unresolved microimages. Specifically, the estimated cross section  $\sigma$  can be related to  $A$  via

$$\sigma(\delta; \kappa, \gamma, \beta) = \left| \frac{\det(1 - \beta\Gamma)}{\det(1 - \Gamma)} \right| A(\delta; \kappa_{\text{eff}}, \gamma_{\text{eff}}), \quad (4)$$

where the matrix  $\Gamma$  is,

$$\Gamma = \begin{bmatrix} \kappa + \gamma & 0 \\ 0 & \kappa - \gamma \end{bmatrix}. \quad (5)$$

The area  $A$  is a function of  $\delta, \kappa$ , and  $\gamma$ , where the convergence and shear are modulated by the difference in redshift between the lens and the clump. The effective values of the convergence and shear are

$$\kappa_{\text{eff}} = \frac{(1 - \beta)[\kappa - \beta(\kappa^2 - \gamma^2)]}{(1 - \beta\kappa)^2 - (\beta\gamma)^2} \quad (6)$$

and

$$\gamma_{\text{eff}} = \frac{(1 - \beta)\gamma}{(1 - \beta\kappa)^2 - (\beta\gamma)^2}. \quad (7)$$

The functional form of  $A$  depends on the global parity of the image (see Keeton 2003, eqns. 11, 15, 17, and 18 for specific forms). For a negative parity image, the result is different for positive and negative perturbations. Typically, the optical depth for the  $\delta < 0$  case is much larger than the  $\delta > 0$  optical depth, so clumps tend to make negative-parity images dimmer.

The dependence of the cross section on the mass of the clump is simple and is contained within a factor of the Einstein radius squared, i.e.,  $\sigma \propto A \propto b^2(M)$ . For halos with a SIS density distribution, the Einstein radius is given by a simple expression:

$$b = 4\pi \left( \frac{\sigma_{\text{rms}}}{c} \right)^2 \frac{D_{ls}}{D_{os}}, \quad (8)$$

where  $\sigma_{\text{rms}}$  is the velocity dispersion of the halo,  $c$  is the speed of light, and  $D_{ls}$  and  $D_{os}$  are the angular diameter distances between the lens and the source and the observer and the source, respectively. Due to the relative simplicity of the SIS profile and corresponding expressions, we assume SIS cross-sections in our analysis. Although SIS profiles do not describe the density distributions of cosmological halos, this assumption is reasonable for our purposes, since the density distribution of total mass (baryons and DM) in the centers of galaxies is close to isothermal. Also, at this point we are primarily interested in evaluating the *relative* contributions of field clumps and substructure rather than evaluating the absolute optical depth. Here we only note that the internal density distribution of substructure halos is still uncertain and we are currently investigating it using numerical simulations. The analysis presented in this paper can be easily extended for other profiles.

## 3. POPULATIONS OF DARK MATTER HALOS

We model the cosmological populations of dark matter halos by separating halos into three distinct categories: 1)

*substructure* or halos located within the virial radius of the lens halo; 2) *halos in the vicinity of the lens*: halos that are located outside the virial radius but in the immediate vicinity of the lens; and 3) *isolated* halos or halos that are located far from the lens. For the latter halos, we assume a number density given by the average cosmological halo mass function. We do not take into account substructure in other halos that projects onto the lens. This is a reasonable assumption the strong lenses analyzed in the literature usually have no apparent bright host projecting near the lens. At the same time, in cases where a bright galaxy is seen near the lens, it is included in the smooth mass model. Below we describe in detail how each halo category was modeled. Throughout the paper, we assume the currently favored flat  $\Lambda$ CDM cosmology with the following parameters:  $h = 0.65$ ,  $\Omega_M=0.35$ ,  $\Omega_\Lambda=0.65$ , and the power spectrum normalization of  $\sigma_8=0.92$  (the *rms* variance of mass distribution on the scale of  $8h^{-1}$ Mpc).

### 3.1. Substructure Halos

The substructure halo population is assumed to have a power-law mass function,

$$\frac{dn}{dm} \propto m^{-\alpha}, \quad (9)$$

with  $\alpha$  in the range of  $1.7 - 1.9$ , as measured in high-resolution cosmological simulations (Ghigna et al. 2000). The spatial distribution of the substructure halos is assumed to follow that of dark matter: i.e., their spherically averaged number density profile is assumed to be described by a NFW profile (Navarro et al. 1997) outside of a core radius  $r_c$  and constant or zero inside the core radius:

$$\frac{dn}{dm} \propto \begin{cases} (r/r_s)^{-1} (1 + r/r_s)^{-2}, & r > r_c \\ \rho(r_c) \text{ or } 0, & r \leq r_c. \end{cases} \quad (10)$$

This model is based on the results of high-resolution cosmological simulations (Colin et al. 1999; Ghigna et al. 2000; Kravtsov et al. 2003). However, we should note that predictions for the spatial distribution of substructure in the innermost ( $\lesssim 0.1R_{\text{vir}}$ ) regions of halos may still suffer from “overmerging” (see discussion in § 6). As we will show below, our results are very sensitive to the assumptions about the radial distribution of substructure halos and this aspect of the model is one of its largest uncertainties.

The characteristic inner radius is given by  $r_s = R_{\text{vir}}/c_{\text{vir}}$ , where  $R_{\text{vir}}$  is the virial radius of the lens halo corresponding to an overdensity of  $\Delta = 340$  and  $c_{\text{vir}}$  is the concentration parameter as given by Bullock et al. (2001), as a function of mass and redshift

$$c_{\text{vir}} = \frac{9}{1 + z_l} \left( \frac{M_{\text{vir}}}{M_*} \right)^{-0.13}, \quad (11)$$

where  $M_*$  is defined as  $\sigma(M_*) = \delta_c = 1.686$ , and  $z_l$  is redshift of the lens halo. The relation (9) is normalized by assuming that a certain fraction,  $f_{\text{sub}}$ , of the virial mass of the lens is associated with substructure and setting minimum and maximum limits for substructure halo masses. The normalization constant,  $K$ , for the relation is dependent upon the mass limits, such that

$$K \propto [M_{\text{max}}^{2-\alpha} - M_{\text{min}}^{2-\alpha}]. \quad (12)$$

The minimum mass,  $M_{\text{min}}$ , is set to be very small and has a negligible effect on our results for mass function slopes

of  $\alpha < 2$  (it would, of course, be important for  $\alpha = 2$ ). For slopes that approximate the mass functions of substructure in high-resolution simulations,  $\alpha \approx 1.7 - 1.9$ , the normalization is sensitive only to the maximum substructure mass,  $M_{\text{max}}$ . For our fiducial model (§ 3.4) we assume that  $M_{\text{max}}$  is equal to 0.01 of the host mass. In cosmological simulations,  $M_{\text{max}}$  is typically found to be  $\sim 0.01 - 0.05$ . Satellites of larger mass are expected to merge with the host very quickly after accretion due to dynamical friction. In addition, in lens modelling the most massive satellites are usually incorporated as part of the smooth mass models. We explore the sensitivity of the results to  $M_{\text{max}}$  below (see Fig. 2).

As satellites accrete onto the lens galaxy, the matter in their outer portions is tidally stripped. We approximate the tidal radius as the radius at which the density of the clump equals the local density of the lens halo. The velocity dispersions are assumed to remain unchanged. Thus, the mass,  $M$ , for the substructure halos in eq. 9 is the mass within the tidal radius. This is taken into account in calculating the Einstein radius and determining the mass limits of integration.

Figure 1 compares the number density profile of substructure halos predicted in our model to the number density profile measured in a high-resolution cosmological simulation of a galaxy-sized DM halo (one of the three halos analyzed in Klypin et al. 2001). The halo was simulated in the flat  $\Lambda$ CDM cosmology ( $\Omega_m = 0.3$ ,  $h = 0.7$ ,  $\sigma_8 = 0.9$ ) and the profile measured at  $z = 0.176$ , typical for lens halos. At this epoch, the mass of the halo is  $M_{180} = 1.34 \times 10^{12} h^{-1} M_\odot$  and the most massive substructure halo has a mass of  $M_{\text{max}} = 2.76 \times 10^{10} h^{-1} M_\odot$ . We include only halos with  $M > M_{\text{min}} = 2.0 \times 10^7 h^{-1} M_\odot$ , which corresponds to the completeness limit of the halo catalogs in the simulation. The mass fraction in substructure halos within the virial radius for this halo is  $f_{\text{sub}} = 0.087$ .

The figure shows that the agreement between our model and the simulation result is good at large radii. At small radii, however, the density of substructure halos is overestimated in the fiducial model; the simulation profile is much better approximated by a model with a larger value of  $r_c$ . However, the simulation may actually underestimate the abundance of substructure in the inner regions due to limited mass and force resolution (see also § 6). We have chosen the fiducial model conservatively, possibly overestimating the effects of substructure. We estimate the effect of different assumptions about the number density profile of substructure in § 5. If it turns out that substructure abundance has been overestimated our conclusions about importance of isolated halos will be strengthened.

### 3.2. Halos around the lens

The number density profile of halos outside the virial radius but in the immediate vicinity of the lens are accounted for in the calculation using the cross-correlation function

$$n_m(r) = \bar{n}_m [1 + b_{M_l} b_m \xi_{dm}(r)], \quad (13)$$

where subscript  $m$  indicates the number density of objects of mass  $m$ ,  $b_{M_l}$  and  $b_m$  are the bias for the lens halo and clump, respectively, and  $\bar{n}_m$  is the average cosmological density of halos of mass  $m$  (eq. 15). We use expressions

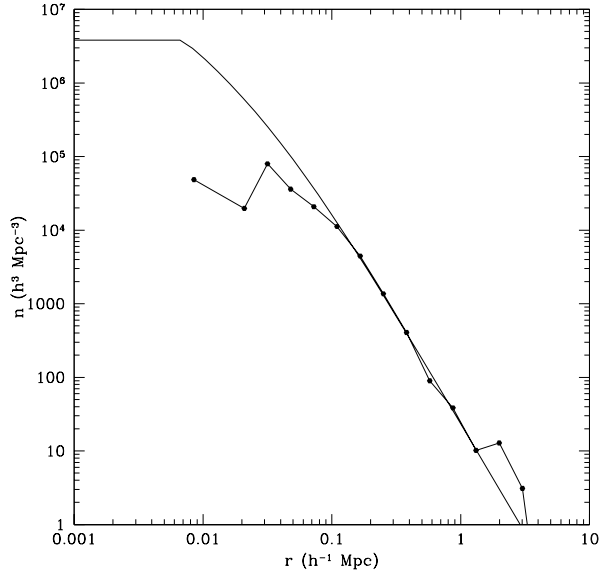


FIG. 1.— The number density profile of substructure halos predicted in our model (§ 3.1) compared to the number density profile measured in a high-resolution cosmological simulation of a galaxy-size DM halo. The halo was simulated in the flat  $\Lambda$ CDM cosmology ( $\Omega_m = 0.3$ ,  $h = 0.7$ ,  $\sigma_8 = 0.9$ ) and the profile measured at redshift  $z = 0.176$ , typical for lens halos. At this epoch, the mass of the halo is  $M_{180} = 1.34 \times 10^{12} h^{-1} M_\odot$  and the most massive substructure halo has a mass of  $M_{\max} = 2.76 \times 10^{10} h^{-1} M_\odot$ . We include only halos with  $M_{\max} > M > M_{\min} = 2.0 \times 10^7 h^{-1} M_\odot$ , which corresponds to the completeness limit of the halo catalogs. The figure shows that the agreement between our model and simulation result is good at large radii. At small radii, however, the density of substructure halos is overestimated in the fiducial model; the simulation profile is much better approximated by a model with a larger value of  $r_c$ .

for the bias and the mass function from Sheth & Tormen (1999) (see § 3.3 for details) and the fitting formula of Peacock & Dodds (1996) to calculate the nonlinear dark matter correlation function  $\xi_{dm}(r)$ . Masses outside of the lens virial radius are assumed to correspond to masses of overdensity  $\Delta = 178$  as in Sheth & Tormen (1999). The above expression is integrated for the mass limits assumed in the calculation (see § 3.4). The total number density of dark matter halos as a function of radius  $n(r)$  is then the maximum of the number density from the lens substructure model (eqs. 9 and 10) and the number density given by eq. 13 (see Fig. 3).

We should note that the adopted model may overestimate the optical depth of halos within and in the vicinity of *isolated galaxy-mass* lenses. The equation 13 estimates the density profile around an average halo, including halos in very dense regions such as clusters. Thus, the average profile  $n_m(r)$  may be higher than that of a relatively isolated halo. Since many lenses are found in groups and clusters (Keeton et al. 2000), and the two specific lenses we focus on here are located in galaxy groups,  $n_m(r)$  should provide a representative profile.

We find the optical depth by integrating the volume element for the satellite halos – both substructure halos and nearby halos – over a cylinder in Euclidean geometry, centered around the position of the image, integrating through the halo out to a radius of  $10h^{-1}$  Mpc. The optical depth

equation, (1), then becomes

$$\tau = D_{ol}^2 \int dx \int dM \frac{dn}{dM}(M, x) \sigma(M). \quad (14)$$

### 3.3. Isolated Halos

For the population of isolated halos we assume a uniform spatial distribution with a mass function which reasonably fits both the low mass and high mass ends of the mass function of halos identified in numerical simulations of CDM models. Specifically, we use the analytic mass function of Sheth & Tormen (1999)

$$\frac{dn}{d \ln M} = \frac{\rho}{M} \frac{d \ln \sigma^{-1}}{d \ln M} f(\sigma), \quad (15)$$

where

$$f(\sigma) = A \sqrt{\frac{2a}{\pi}} \left[ 1 + \left( \frac{\sigma^2}{a\delta_c^2} \right)^p \right] \frac{\delta_c}{\sigma} \exp\left(-\frac{a\delta_c^2}{2\sigma^2}\right), \quad (16)$$

$A=0.3222$ ,  $a=0.707$ ,  $p=0.3$ , and  $\delta_c=1.686$ . We use the fitting formula for the transfer function provided by Eisenstein & Hu (1999) and a spherical top hat window function for the mass variance. As we noted above, all the halos are modeled as isothermal spheres, where the masses of the clumps are defined as in Sheth & Tormen (1999) to be the mass within the radius at which the overdensity is  $\Delta=178$ .

To get the number of projected isolated clumps, we integrate over the comoving volume from  $z = 0$  to the redshift of the source and over the assumed mass limits for small-mass clumps:

$$\tau = \int_0^{z_s} dz D(z)^2 \frac{dD}{dz} \int dM \frac{dn}{dM}(M, z) \sigma(M, z). \quad (17)$$

### 3.4. Fiducial Model

In our fiducial model, we set the magnification perturbation to  $\delta = 0.2$ , i.e., calculating the cross section for perturbations greater than 20%. The mass limits for halos outside the virial radius of the lenses are assumed to be  $10^{-10} \times M_{vir}$  to  $0.1 \times M_{vir}$ , where  $M_{vir}$  denotes the virial mass of the lens. Given that halos in a lens galaxy which pass close to the lens center are typically stripped of  $\sim 90\%$  of their mass by the tidal field of the host after 1-2 orbits (e.g., Klypin et al. 1999a; Hayashi et al. 2002), the upper limit on substructure masses is assumed to be 0.1 of that for the isolated clumps, i.e.,  $0.01 \times M_{vir}$ . The core radius of the substructure number density profile is assumed to be  $r_c = 10$  kpc with a constant number density interior to it, the slope of the mass function is set to  $\alpha = 1.8$ , and the fraction of mass in substructure is assumed to be  $f_{sub} = 0.1$ . The value of  $f_{sub}$  is close to the upper end of the range found in cosmological simulations and maximizes the normalization of the mass function and the optical depth due to substructure. The sensitivity of the results to  $M_{\max}$ ,  $f_{sub}$ , and  $\alpha$  is shown in Figure 2 and will be discussed in § 6.

## 4. LENS PARAMETERS

We estimate lensing cross-sections for two specific cases of quadruple-image gravitational lenses in which flux anomalies have been detected: B1422+231 and PG 1115+080. The source B1422+231 is a radio-loud quasar at  $z=3.62$

TABLE 2  
LENSING OPTICAL DEPTH DUE TO DIFFERENT HALO POPULATIONS

Lens/Image	$\tau_{\text{sub}}$	$\tau_{<10} - \tau_{\text{sub}}$	$\tau_{>10}$	$\tau_{>10}/\tau_{<10}$
B1422+231				
A	1.8	$1.9 \times 10^{-3}$	$4.5 \times 10^{-2}$	$2.5 \times 10^{-2}$
B ( $\delta < 0$ )	2.8	$2.8 \times 10^{-3}$	$2.1 \times 10^{-2}$	$7.6 \times 10^{-3}$
( $\delta > 0$ )	$6.5 \times 10^{-3}$	$6.7 \times 10^{-6}$	$4.2 \times 10^{-3}$	0.65
C	0.76	$8.2 \times 10^{-4}$	$2.8 \times 10^{-2}$	$3.7 \times 10^{-2}$
D ( $\delta < 0$ )	$1.1 \times 10^{-3}$	$7.6 \times 10^{-7}$	$3.4 \times 10^{-7}$	$3.2 \times 10^{-4}$
( $\delta > 0$ )	$2.9 \times 10^{-2}$	$2.1 \times 10^{-5}$	$1.0 \times 10^{-2}$	0.35
PG 1115+080				
A <sub>1</sub>	15.	$1.0 \times 10^{-2}$	$8.3 \times 10^{-2}$	$5.6 \times 10^{-3}$
A <sub>2</sub> ( $\delta < 0$ )	14.	$1.0 \times 10^{-2}$	$5.6 \times 10^{-2}$	$4.0 \times 10^{-3}$
( $\delta > 0$ )	$1.1 \times 10^{-2}$	$7.6 \times 10^{-6}$	$6.6 \times 10^{-4}$	$6.2 \times 10^{-2}$
B ( $\delta < 0$ )	0.41	$2.7 \times 10^{-4}$	$9.3 \times 10^{-4}$	$2.3 \times 10^{-3}$
( $\delta > 0$ )	$2.3 \times 10^{-2}$	$1.5 \times 10^{-5}$	$1.5 \times 10^{-3}$	$6.5 \times 10^{-2}$
C	0.88	$7.0 \times 10^{-4}$	$9.6 \times 10^{-3}$	$1.1 \times 10^{-2}$

TABLE 1  
LENS PARAMETERS

Lens/Image	$\kappa$	$\gamma$	$\mu$	image position (")
B1422+231				
A	0.384	0.476	6.57	1.014
B	0.471	0.634	-8.26	0.961
C	0.364	0.414	4.29	1.056
D	1.863	2.025	-0.30	0.284
PG 1115+080				
A <sub>1</sub>	0.532	0.412	19.96	1.173
A <sub>2</sub>	0.551	0.504	-19.10	1.120
B	0.663	0.644	-3.32	0.950
C	0.469	0.286	5.00	1.397

Note –  $\kappa$ ,  $\gamma$ ,  $\mu$  are the convergence, shear, and parity of the images, respectively, from macromodels. B1422+231 is modeled as a singular isothermal ellipsoid (SIE) plus an external shear (Keeton 2001). PG 1115+080 is modeled as a SIE plus an additional SIS representing the surrounding poor group of galaxies (Impey et al. 1998).

lensed by an early-type galaxy in a poor group of galaxies at  $z=0.34$  (Patnaik et al. 1992; Kundic et al. 1997b; Tonry 1998). Images A and C are bright positive-parity images, parity corresponding to the sign of the magnification, while image B is a bright negative-parity image and D is a faint negative-parity image (Patnaik et al. 1999). Keeton (2001) and Bradač et al. (2002) recently argued that a clump projecting in front of the image A can fit the lens data, concluding that mass of the perturber should be of order  $\sim 10^{5-6} M_{\odot}$  if it is a point mass, or  $\sim 10^{6-7} M_{\odot}$  if the mass distribution is extended (i.e., a halo) with a SIS density distribution.

PG 1115+080 is a radio-quiet quasar at  $z=1.72$  lensed by an early-type galaxy in a poor group of galaxies at  $z=0.31$  (Weymann et al. 1980; Kundic et al. 1997a; Tonry

1998). Images A<sub>1</sub> and C are positive-parity images, while A<sub>2</sub> and D are negative-parity images (Impey et al. 1998). Smooth lens models for PG 1115+080 are able to fit all but the A<sub>1</sub>/A<sub>2</sub> flux ratio. Table 1 summarizes the properties of the observed images in these studies relevant to our study. The concentration parameter for B1422+231 is 7.9, while that of PG 1115+080 is 7.3. The concentration parameters are estimated using eq. 11 for the virial mass of the lens and its redshift. The mass, in turn, is derived from the lens model. Namely, we use the estimate of the Einstein radius from the lens velocity dispersion and invert eq. 8. The virial mass is then calculated assuming an isothermal profile as the mass within the radius corresponding to overdensity of  $\Delta=340$ . The estimates of the virial mass and the Einstein radius of B1422+231 is  $5.1 \times 10^{12} M_{\odot}$  and  $0.764''$  (Keeton 2001), while those of PG 1115+080 are  $1.1 \times 10^{13} M_{\odot}$  and  $1.147''$  (Impey et al. 1998).

## 5. RESULTS

Using the model described in the previous sections, we calculate and compare the lensing optical depths due to the substructure halos,  $\tau_{\text{sub}}$ ; due to all halos within  $r < 10h^{-1}$  Mpc of the lens,  $\tau_{<10}$  (this optical depth includes both substructure and halos in the vicinity of the lens); and due to all 'field' halos along the line of sight from the source to the observer but excluding halos within  $10h^{-1}$  Mpc of the lens,  $\tau_{>10}$ .

Table 2 compares  $\tau_{\text{sub}}$ ,  $\tau_{<10}$ , and  $\tau_{>10}$  for our fiducial model. The table shows that in the fiducial case the substructure halos provide a dominant contribution to the lensing optical depth for all images. The contribution of nearby clumps outside the virial radius of the lens (i.e.,  $\tau_{<10} - \tau_{\text{sub}}$ ) is negligible. The optical depth due to isolated clumps along the line of sight,  $\tau_{>10}$ , is generally small compared to the substructure optical depth (a few percent) for all positive parity images. In negative parity images, the relative effect for magnification is much larger. Magnification, however, is a much smaller effect than de-magnification in these images. Thus, the contri-

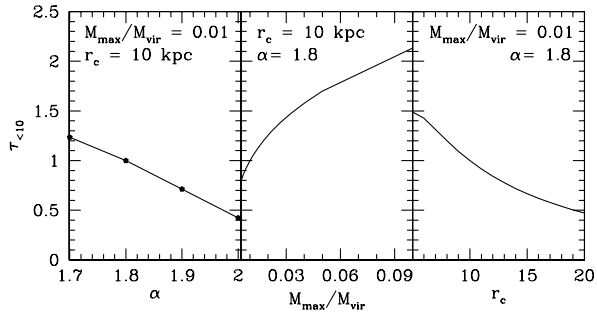


FIG. 2.— The effect of varying  $\alpha$ , the upper mass limit  $M_{\max}$ , and the core radius,  $r_c$ , on the optical depth of satellites is shown here from left to right for B1422+231, image A, where the optical depth is normalized to  $\tau=1$  for the fiducial values. In each case, all other parameters of the model are kept fixed at their fiducial values.

bution of isolated halos is relatively small. It is, however, not negligible and should be included in detailed analyses of substructure lensing.

The results of the full numerical model can be recovered using simple analytic estimates. The substructure optical depth can be estimated as (c.f. eq. 14)

$$\tau_{\text{sub}} \approx D_{\text{ol}}^2 \Delta x \left[ \frac{dn}{dM}(M_{\text{eff}}) \right] \Delta M \sigma(M_{\text{eff}}), \quad (18)$$

where  $\Delta M \approx M_{\text{eff}}$ . Given that the substructure optical depth ought to be of order unity, we can use this equation to estimate the effective mass. For B1422+231,  $M_{\text{eff}} \sim 10^8 M_{\odot}$ , where  $M_{\text{eff}}$  is a tidally truncated mass. The corresponding virial mass of isolated halos would then be  $M_{\text{eff}}^{\text{iso}} \sim 10^9 M_{\odot}$ . We can thus estimate the relative importance of the line-of-sight optical depth (c.f. eq. 17):

$$\tau_{>10} \approx \Delta D D_{\text{ol}}^2 \left[ \frac{dn}{dM}(M_{\text{eff}}^{\text{iso}}, z_l) \right] \Delta M \sigma(M_{\text{eff}}^{\text{iso}}, z_l), \quad (19)$$

where for  $\Delta z \sim 0.3 - 0.5$  (the wings of the lensing cross section),  $\Delta D \sim D_{\text{ol}}$ . Rewriting the equation explicitly in term of mass,

$$\tau_{>10} \approx 1.6 \times 10^{-25} D_{\text{ol}}^3 \left[ \frac{dn}{dM}(M_{\text{eff}}, z_l) \right] M_{\text{eff}}^{7/3}. \quad (20)$$

For B1422+231 and the given effective mass of  $M_{\text{eff}} \sim 10^9 M_{\odot}$ ,  $D_{\text{ol}} \sim 10^3$  Mpc and  $\frac{dn}{dM}(M_{\text{eff}}) \sim 10^{-9}$ ,  $\tau_{>10} \sim 10^{-4}$ . The optical depth is  $\tau \sim M_{\text{eff}}^{1/2}$ , so for  $M_{\text{eff}} = 10^{11} M_{\odot}$  the optical depth is  $\tau \approx 10^{-3}$ , roughly consistent with our numerical results. The total optical depth is a sum of the contributions by halos of different masses. This exercise shows, however, that most of the signal for the model we adopted is due to the high-mass end of the halo mass function.

The relative contribution of isolated halos could be larger, if the fiducial model overestimates the abundance of substructure halos. Below we discuss the sensitivity of the optical depth calculations to our model parameters. The optical depth  $\tau_{\text{sub}}$  depends on the assumed slope of the halo mass function,  $\alpha$ ; the mass limits,  $M_{\min}$  and  $M_{\max}$ ; the mass fraction in substructure,  $f_{\text{sub}}$ ; and the assumed shape of the radial number density profile. The lensing cross section  $\sigma$  is proportional to the square of the Einstein radius, which, for SIS halos, implies

$$\sigma \propto m^{4/3}. \quad (21)$$

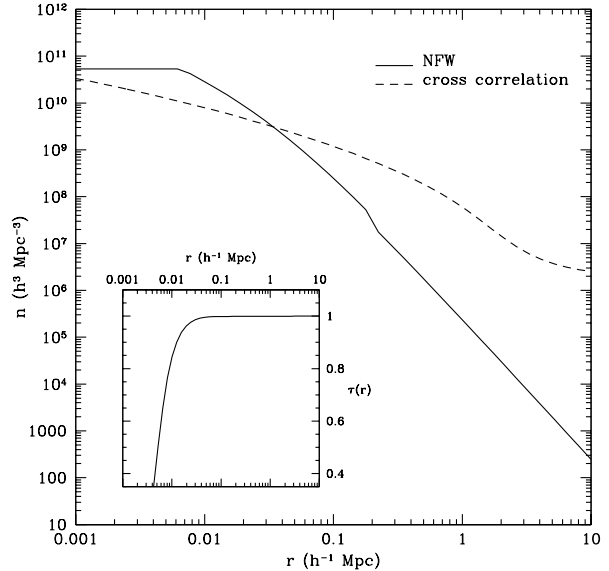


FIG. 3.— The number density profile for the image A of lens B1422+231. The two lines show the profile for substructure halos (eq. 10, solid line) with fiducial model parameters and the profile for the halos in the vicinity of the lens (eq. 13, dashed line). The break in the profile of the substructure halos at  $\approx 200 h^{-1}$  kpc (the virial radius) is due to change of mass from tidally truncated to virial (for halos outside the virial radius of the lens) in our model. The corresponding optical depth profile is inset.

Since the mass function of small-mass DM clumps is approximated by a power-law  $n \propto m^{-\alpha}$ , we have

$$\frac{d\tau}{dm} \propto m^{4/3-\alpha}, \quad \tau \propto \left[ M_{\max}^{7/3-\alpha} - M_{\min}^{7/3-\alpha} \right]. \quad (22)$$

For  $\alpha = 1.7 - 2$ ,  $7/3 - \alpha$  is in the range  $2/3 - 1/3$ , and the value of  $M_{\min}$  is unimportant. For the fiducial case,  $\alpha = 1.8$ ,  $\tau_{\text{sub}} \propto M_{\max}^{8/15}$ . The dependence on  $f_{\text{sub}}$  is simple:  $\tau_{\text{sub}} \propto f_{\text{sub}}$ .

The constraints on substructure masses for B1422+231 suggest that the fluxes of this lens can only be affected by masses,  $M \geq 10^6 M_{\odot}$  (Keeton 2001; Bradač et al. 2002). Thus, masses below this value but above the minimum mass, should have little effect on the optical depth. The substructure optical depth for image A of the system for masses between  $M_{\min}$  and  $10^6 M_{\odot}$  is  $\tau_{\text{sub}} = 0.005$ , or 0.3% of the total optical depth. The optical depth for masses between  $M_{\min}$  and  $10^7 M_{\odot}$  is  $\tau_{\text{sub}} = 0.02$ , or 1% of the total, calculated optical depth.

The fiducial value of  $f_{\text{sub}} = 0.1$  is typical for CDM halos. Although  $f_{\text{sub}}$  varies from halo to halo, variations of more than a factor of  $\sim 2 - 3$  from the fiducial model are expected to be rare (Kravtsov et al. 2003). Nevertheless, in the case when  $f_{\text{sub}}$  and  $M_{\max}$  are at the lower end of the range expected for CDM halos the optical depth can be reduced by a factor of  $\sim 2$ . Note that these parameters are not independent. For example, for  $\alpha < 2$  lower  $M_{\max}$  will correspond to lower  $f_{\text{sub}}$ .

Figure 2 shows the effect of varying  $\alpha$ ,  $M_{\max}$ , and the core radius,  $r_c$ , on the optical depth due to nearby and substructure halos relative to the fiducial model. The figure shows that varying the mass function slope  $\alpha$  has relatively small effect: less than a factor of 2 for a realistic range of values. The variation of  $M_{\max}$  (for  $\alpha = 1.8$ ) results in only

a factor of  $\sim 2 - 3$  change in optical depth. In the case where we model the substructure number density profile as described in § 3.1, our only variable parameter is  $r_c$ , which also varies the optical depth by a factor of  $\sim 2 - 3$ . Thus, our results are not expected to change drastically due to variations of  $\alpha$ ,  $r_c$ , and  $M_{\text{max}}$ . The optical depth profile, however, is also affected, which we discuss below, and the shape of the radial number density profile is not well-constrained in cosmological simulations.

Figure 3 shows the number density profile of clumps inside and in the immediate vicinity of the halo of lens B1422+231; the inset shows the cumulative optical depth profile for image A, which is likely to have substructure affecting its flux. The profile is normalized to unity and does not include the effect of isolated halos outside  $10h^{-1}$  Mpc. The figure shows that most of the optical depth is contributed by regions of the highest number density. In this particular case, the clumps outside  $\sim 10\%$  of the virial radius contribute  $\lesssim 2\%$  of the optical depth. Clearly, the substructure optical depth is very sensitive to the distribution of DM clumps in the innermost regions of the lens halo. In our model the inner number density of substructure clumps is determined by the core radius  $r_c$ .

Figure 4 shows the optical depth profiles for different values of  $r_c$ . The main panel shows the optical depth  $\tau(r)$  normalized to unity. Here again we see that halos at  $r \lesssim r_c$  contribute most of the signal. The inset panel shows the corresponding unnormalized profiles  $\tau(r)$  and demonstrates that the total optical depth due to substructure is quite sensitive to the inner distribution of clumps. The lowest curve corresponds to the case where no clumps are present within the central 20 kpc. In this case the optical depth is a factor of ten smaller than the optical depth for the fiducial model, which would increase the relative contribution of isolated halos to  $\sim 20\text{-}30\%$  (c.f. Table 2).

## 6. DISCUSSION AND CONCLUSIONS

Substructure in galaxy-sized lens halos, if present, may alter the flux ratios of gravitationally lensed images. Studies of multiply-imaged quasar lenses are therefore a unique probe into the small-scale matter distribution in DM halos and may prove to be one of the most powerful tests of the CDM paradigm. Indeed, two of the most glaring problems for the CDM models are the density distribution in galaxies (predicted halos are too dense and possibly too cuspy) and clusters and the overabundance of small-mass DM clumps. Both problems are a manifestation of the relatively high amplitude of the CDM power spectrum on small scales. If DM clumps can be proven to be a unique explanation for the anomalous flux ratios, this would confirm that the small-scale power is high and would lend support to the view that the problem of density distribution in galaxies has an “astrophysical” solution.

In order to extract useful constraints from lensing observations, we must understand what parameters the lensing is sensitive to and what type of halos may contribute to the total lensing signal. In this paper, we presented results of the first study comparing the lensing optical depths due to small-mass halos within the lens halo (substructure), the halos in the immediate vicinity of the lens, and the overall cosmological population of small-mass halos distributed throughout the entire line of sight between the source and

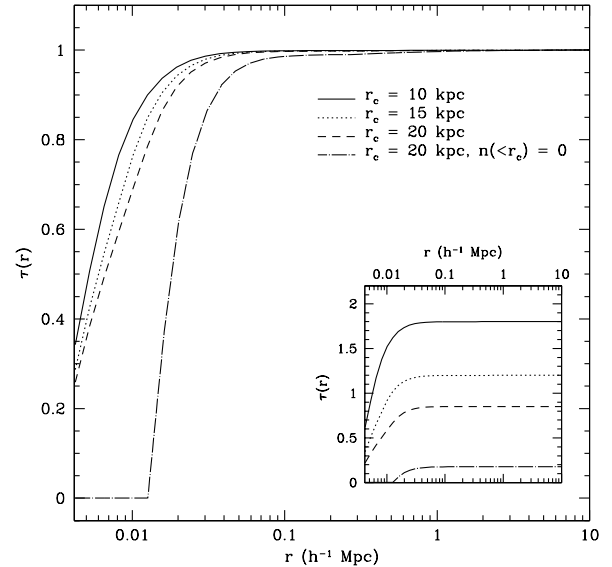


FIG. 4.— The optical depth profile for image A of lens B1422+231 normalized to unity, for different values of  $r_c$ . The solid line is for the fiducial value of  $r_c=10$  kpc, the dashed lines are  $r_c=15$  kpc,  $r_c=20$  kpc, and  $n(r)=0$  when  $r < 20$  kpc, respectively. The unnormalized profiles are inset. The contribution of isolated line-of-sight halos are not included in the optical depth shown here.

the observer.

The main result of our paper is that the dominant contribution to the total lensing optical depth is provided by the DM clumps in the densest, innermost regions of the lens halo. The optical depth is therefore very sensitive to the spatial distribution of substructure clumps within the lens. While the effect of masses near the lens galaxy is more important than elsewhere, the cumulative effect of all the (isolated) halos along the line-of-sight to the source is not negligible. In the  $\Lambda$ CDM universe, we find that the contribution of isolated halos can be a sizeable fraction of the total lensing signal.

The exact percentage of the isolated halo contribution depends sensitively on the mass function of substructure halos and, especially, on their spatial distribution. The latter is currently uncertain in cosmological simulations. In the highest resolution cosmological  $N$ -body simulations reported to date, no clumps are typically found within the central 10% of the virial radius, while at larger radii the number density profile of substructure halos has the shape similar to that of the overall DM profile (Colín et al. 1999; Ghigna et al. 2000; Stoehr 2002; Kravtsov et al. 2003). If such a distribution is assumed in our model, the contribution of isolated halos to the optical depth can be as high as  $\sim 20 - 30\%$ . The degree to which the results of cosmological simulations are affected by resolution is currently unclear. It is possible that in the innermost regions the simulations still suffer from the perennial “overmerging” problem. On the other hand, the tidal disruption of NFW halos by the host is expected (Klypin et al. 1999a; Hayashi et al. 2002). In addition, clumps in real lenses would experience enhanced tidal forces due to the baryonic material in the center of the lens which would make their destruction more efficient than in  $N$ -body simulations, and so the

lack of halos in the central 10% of the virial radius may be a real effect.

Our results imply that flux ratio anomalies, if caused by DM clumps, do indeed probe the substructure population of lens halos and are a very promising test of CDM predictions on small-scales. For example, the alternative scenarios proposed to remedy perceived CDM problems, such as the simplest variants<sup>2</sup> of self-interacting DM (SIDM Spergel & Steinhardt 2000) and warm DM (WDM, e.g. Colín et al. 2000; Bode et al. 2001) predict a very reduced abundance of substructure halos and, thus, a lower lensing optical depth compared to that from the CDM models.

Our estimates for the optical depth in the  $\Lambda$ CDM halos are in the range of  $\sim 0.2 - 20$  and could naturally explain the high-frequency of anomalous flux ratio images. In contrast, SIDM and WDM models would have optical depths of  $\tau \lesssim 0.1$ , although detailed calculations are needed. In addition in WDM and SIDM scenarios, lensing by isolated halos and by substructure would have comparable optical depths because we do not expect a significant change in the abundance of isolated halos in these models. To be precise, WDM models predict that abundances should be suppressed below a mass scale that corresponds to the scale of the power spectrum cut-off. The suppression is applicable for both isolated and substructure halos. However, for substructure halos the abundance is further decreased by tidal disruption, while the abundance of the field halos may be increased due to fragmentation (e.g., Colín et al. 2000; Bode et al. 2001; Knebe et al. 2003). So we expect that the contribution of isolated halos would be even more important in the WDM models than in  $\Lambda$ CDM.

We should also note that our results imply that precise cosmological constraints, such as estimates of the WDM particle mass or of the cross-section of the SIDM interaction, are difficult if not impossible to derive at this point. As shown in our analysis, isolated field halos can contribute a sizeable fraction to the lensing optical depth. Also, the ingredients that are needed to estimate relative effects of substructure and isolated halos in various models are still rather uncertain. Even in the relatively well studied  $\Lambda$ CDM cosmology, the distribution of DM clumps in the innermost regions of halos is not well understood. In particular, simulations which include the effects of baryons (a disk or stars in an elliptical galaxy) on the tidal disruption of DM clumps are only starting to be employed (e.g., Bradač et al. 2002). Even for isolated halos the Sheth & Tormen (1999) mass function that we used in our calculations has been tested only down to  $M \sim 10^{10} h^{-1} M_{\odot}$  (Reed et al. 2003). Given the importance of the problem, these issues should and will be addressed in the next generation of cosmological simulations. Significant progress in determining properties of substructure halos and the mass function of field populations in the last several years makes us optimistic that uncertainties will be resolved in the near future.

We would like to thank Neal Dalal, Daniel Holz, Anatoly Klypin, Andrew Zentner, and James Bullock for useful discussions and the anonymous referee for construc-

tive comments. This work was partially supported by the grant AST-0206216 from the National Science Foundation (NSF). C.R.K. is supported by NASA through Hubble Fellowship grant HST-HF-01141.01-A from the Space Telescope Science Institute, which is operated by the Association of Universities for Research in Astronomy, Inc., under NASA contract NAS5-26555.

## REFERENCES

- Benson, A. J., Lacey, C. G., Baugh, C. M., Cole, S., & Frenk, C. S. 2002, *MNRAS*, 333, 156
- Bergström, L., Edsjö, J., Gondolo, P., & Ullio, P. 1999, *Phys. Rev. D*, 59, 43506
- Bode, P., Ostriker, J. P., & Turok, N. 2001, *ApJ*, 556, 93
- Bradač, M., Schneider, P., Steinmetz, M., Lombardi, M., King, L. J., & Porcas, R. 2002, *A&A*, 388, 373
- Bullock, J. S., Kolatt, T. S., Sigad, Y., Somerville, R. S., Kravtsov, A. V., Klypin, A. A., Primack, J. R., & Dekel, A. 2001, *MNRAS*, 321, 559
- Bullock, J. S., Kravtsov, A. V., & Weinberg, D. H. 2000, *ApJ*, 539, 517
- Colín, P., Avila-Reese, V., & Valenzuela, O. 2000, *ApJ*, 542, 622
- Colín, P., Avila-Reese, V., Valenzuela, O., & Firmani, C. 2002, *ApJ*, 581, 777
- Colín, P., Klypin, A. A., Kravtsov, A. V., & Khokhlov, A. M. 1999, *ApJ*, 523, 32
- Dalal, N., & Kochanek, C. S. 2002, *ApJ*, 572, 25
- Eisenstein, D. J., & Hu, W. 1999, *ApJ*, 511, 5
- Evans, N. W., & Witt, H. 2003, *MNRAS*, submitted (astro-ph/0212013)
- Ghigna, S., Moore, B., Governato, F., Lake, G., Quinn, T., & Stadel, J. 2000, *ApJ*, 544, 616
- Hannestad, S., & Scherrer, R. J. 2000, *Phys. Rev. D*, 62, 43522
- Hayashi, E., Navarro, J., Taylor, J., Stadel, J., & Quinn, T. 2002, preprint (astro-ph/0203004)
- Hu, W., Barkana, R., & Gruzinov, A. 2000, *Phys. Rev. Lett.*, 85, 1158
- Impey, C. D., Falco, E. E., Kochanek, C. S., Lehár, J., McLeod, B. A., Rix, H.-W., Peng, C. Y., & Keeton, C. R. 1998, *ApJ*, 509, 551
- Keeton, C. R. 2001, preprint (astro-ph/0111595)
- 2003, *ApJ*, 584, 664
- Keeton, C. R., Christlein, D., & Zabludoff, A. I. 2000, *ApJ*, 545, 129
- Klypin, A., Gottlöber, S., Kravtsov, A. V., & Khokhlov, A. M. 1999a, *ApJ*, 516, 530
- Klypin, A., Kravtsov, A. V., Bullock, J. S., & Primack, J. R. 2001, *ApJ*, 554, 903
- Klypin, A., Kravtsov, A. V., Valenzuela, O., & Prada, F. 1999b, *ApJ*, 522, 82
- Knebe, A., Devriendt, J., Gibson, B., & Silk, J. 2003, submitted (astro-ph/0302443)
- Kravtsov, A. V., Klypin, A., & Gottlöber, S. 2003, in preparation
- Kundic, T., Cohen, J. G., Blandford, R. D., & Lubin, L. M. 1997a, *AJ*, 114, 507
- Kundic, T., Hogg, D. W., Blandford, R. D., Cohen, J. G., Lubin, L. M., & Larkin, J. E. 1997b, *AJ*, 114, 2276
- Mao, S., & Schneider, P. 1998, *MNRAS*, 295, 587
- Mayer, L., Moore, B., Quinn, T., Governato, F., & Stadel, J. 2002, *MNRAS*, 336, 119
- Metcalf, R. B., & Madau, P. 2001, *ApJ*, 563, 9
- Metcalf, R. B., & Zhao, H. 2002, *ApJ*, 567, L5
- Moore, B., Ghigna, S., Governato, F., Lake, G., Quinn, T., Stadel, J., & Tozzi, P. 1999, *ApJ*, 524, L19
- Navarro, J. F., Frenk, C. S., & White, S. D. M. 1997, *ApJ*, 490, 493
- Patnaik, A. R., Browne, I. W. A., Walsh, D., Chaffee, F. H., & Foltz, C. B. 1992, *MNRAS*, 259, 1P
- Patnaik, A. R., Kembell, A. J., Porcas, R. W., & Garrett, M. A. 1999, *MNRAS*, 307, L1
- Peacock, J. A., & Dodds, S. J. 1996, *MNRAS*, 280, L19
- Reed, D., Gardner, J., Quinn, T., Fardal, M., G., L., & Governato, F. 2003, astro-ph/0301270
- Sheth, R. K., & Tormen, G. 1999, *MNRAS*, 308, 119
- Somerville, R. S. 2002, *ApJ*, 572, L23
- Spergel, D. N., & Steinhardt, P. J. 2000, *Phys. Rev. Lett.*, 84, 3760
- Stoehr, F. 2002, private communication
- Tasitsiomi, A., & Olinto, A. V. 2002, *Phys. Rev. D*, 66, 83006
- Tonry, J. L. 1998, *AJ*, 115, 1
- Weymann, R. J., Latham, D., Roger, J., Angel, P., Green, R. F., Liebert, J. W., Turnshek, D. A., Turnshek, D. E., & Tyson, J. A. 1980, *Nature*, 285, 641

<sup>2</sup> More sophisticated SIDM models in which interaction cross-section varies with particle velocity may produce substructure populations similar to those of the CDM models (Colín et al. 2002).